Convective instabilities in complex systems with partly free surface

Dietrich Schwabe

1. Physikalisches Institut der Justus-Liebig-Universität Giessen, H.-Buff-Ring 16, 35392 Giessen, Germany

E-mail: Dietrich. Schwabe@physik.uni-giessen.de

Abstract. Experiments and observations and some selected theoretical studies of thermocapillary instabilities are reviewed. We start with simple idealized model systems of pure thermocapillarity and add to them more complex features like gravity forces, temperature gradients inclined to the free surface, static and dynamic surface deformations, solutocapillary effects and reacting or moving crystal boundaries (like during unidirectional solidification). Many effects and instabilities are demonstrated in video clips which can be downloaded from http://meyweb.physik.uni-giessen.de/1_Forschung/crystalgrowth/video/homepage.html. We try to point out the relationship of thermocapillary instabilities in the more complex systems with those in theoretical studies where the name of these instabilities has been coined.

1 Introduction

1. Outline

This paper deals mainly with surface-tension-driven instabilities like those of thermocapillary flow or the formation of cellular convective structures. It is motivated by the geometries and boundary conditions found in crystal growth from the melt. Therefore, convective effects induced by the large temperature gradients of these crystal growth methods are in the centre of this paper although solutocapillary effects are touched, too. The geometrical and thermal boundary conditions in crystal growth systems can be rather complex, including curved free surfaces like menisci, the combined action of surface tension forces and buoyancy, the presence of moving boundaries (e.g. the growing crystal interface) and the interaction of buoyant-thermocapillary convection with forced convection by crystal rotation in the Czochralski technique. The systems used in melt crystal growth are bounded by walls. Therefore, end-effects and boundary layers need to be considered with their special localized instabilities. Nevertheless, we will start with a review and discussion of unbounded simplified model systems and their instabilities before discussing more complex situations, - adding complexity step by step.

This paper is mainly experimental. The instabilities are demonstrated in video clips and some measurements, but almost never fully characterized because not yet numerically simulated.

The literature on liquid interfacial systems, on their phenomena and instabilities, is vast and not even the special field of this paper can be covered completely. We apologize for having not cited some important work of our colleagues. The reader is referred to the following books [1-6], the review articles [7-8] and the cited original literature which can serve a guides to further problems and further literature.

1.2 Simple models

We consider liquid configurations like layers or vessels with free upper surface or liquid bridges (LBs) and define the following nondimensional groups, e.g. for the case of horizontal liquid layers

aspect ratio	$A = \dfrac{\text{lateral extension L}}{\text{liquid depth d}}$
Prandtl number	$Pr = \nu/\chi$
Rayleigh number	$Ra = g \cdot \beta \cdot \Delta T \cdot d^3 \cdot \nu^{-1} \cdot \chi^{-1}$
horizontal Marangoni number	$Ma_h = \lvert \partial\sigma/\partial T \rvert \cdot (\Delta T_h/L) \cdot d^2 \cdot \eta^{-1} \cdot \chi^{-1}$
vertical Marangoni number	$Ma_v = \lvert \partial\sigma/\partial T \rvert \cdot \Delta T_v \cdot d \cdot \eta^{-1} \cdot \chi^{-1}$
dynamic Bond number	$Bo_{dyn} = Ra/Ma$
surface tension number	$S = \rho \cdot \sigma \cdot d \cdot \eta^{-2}$
capillary number	$Ca = \sigma^{-1} \cdot \lvert \partial\sigma/\partial T \rvert \cdot \Delta T \cdot L^{-1} \cdot d$

with kinematic viscosity ν, dynamic viscosity η, thermal diffusivity χ, surface tension σ, temperature dependence of surface tension $\partial\sigma/\partial T$, volume expansion coefficient β, density ρ, Earth gravity g, temperature difference between the boundaries ΔT. In certain cases one can replace $\Delta T_h/L$ by $\mathrm{grad}_h T$. We denote the bifurcation point by the superscript "c"; e.g. Ra^c is the critical Rayleighnumber. We consider first unbounded (∞-extended) liquid layers with free surface

a) heated from below and cooled from above

b) subject to a horizontal temperature gradient

The basic state of case a) is a stagnant layer, showing a transition to the well-known hexagonal cellular convection pattern [1, 9] of the Bénard-Marangoni-Instability (BMI). (Fig. 1) Pearson [10] analyzed the case excluding gravity and Nield [11] included gravity. The Marangoni effect and buoyant forces reinforce each other lowering the critical Ma or Ra, respectively and influence the pattern (Fig. 2). We find cellular patterns of different type in deep vessels compared to the one in thin layers and again different under microgravity (pure Marangoni effect) (Fig. 3) [12].

For case b) we can consider a linear flow profile without return flow (Fig. 4a) and thermocapillary flow with return flow (Fig. 4b) like Smith and Davis [13]. The basic states of case b) are dynamic layers. The stability analysis of these dynamic layers indicated as most dangerous instability for the linear flow so called linear rolls (roll-axis aligned with the basic flow) and as most dangerous instability of thermocapillary flow with return flow so called hydrothermal waves [13]. The wave vector of the hydrothermal waves is inclined to the applied temperature gradient, the inclination growing with decreasing Pr.

Hydrothermal waves (HTWs) in a thin layer of silicone oil on a metal plate impressing the temperature gradient driving thermocapillarity in rectangular symmetry is shown in Fig. 5 [14]. The HTWs travel from "cold" to "hot" in this experiment as predicted by [13]. For radially oriented temperature gradients like in cylindrical annuli, the HTWs become Archimedian spirals (Fig. 6) for small inner radius because of the angle between wave vector and temperature gradient [15].

Fig. 7 shows an example of HTWs in an open cylindrical annulus with A = 1 under microgravity [16]. The corresponding numerical simulation shows Fig. 8 [17]. The HTWs are found to be travelling azimuthally but as well to form standing waves or waves travelling from one or different sources in opposite direction and interfering (see examples in figure 25 in [18]). The open annulus investigated in [16] and [17] can be taken as a model for a Czochralski crystal growth system, where a crystal (cold cylinder) is grown and pulled out from the free surface of the melt in a crucible (Fig. 9). The main differences to crystal growth are:

- the cold side in the centre is a crystal with the solid-liquid interface at the level of the melt
- the thermal conductivity of the crystal is comparable to that of the melt
- gravity is acting because of large temperature (density) differences
- the free surface is normally strongly cooled because of the high working temperature (high melting points above 1000° C).

The much higher complexity of the Czochralski system will be discussed later.

An example of travelling hydrothermal waves in the meniscus attached to a cooled dummy crystal is shown in Fig. 10 [19]. The HTWs develop only in the range of the cooled crystal because of the largest radial temperature gradient there. They travel well ordered in azimuthal direction. The attempt to damp their amplitude and/or azimuthal travelling speed by counter rotation of the dummy crystal failed; for not too large counter rotation speeds the HTWs change their rotational direction to that of the crystal.

The HTWs do not travel in radial direction in Figs. 7 and 10 compared to Fig. 6. Their travelling direction is only perpendicular to the temperature gradient and not inclined to it as in Fig. 5. The reason for the suppression of the HTW-component parallel to the temperature gradient is the confinement of the HTW to a region near the cold thermal boundary layer with the sufficiently large temperature gradient. Only if the temperature gradient is impressed by a metal bottom with a sufficietly large gradient, HTWs can develop in the whole area of this metal bottom with both wave-components. In case of side-heating and side cooling the HTWs will develop (for $Pr > 1$) only near and in the thermal boundary layers, and with one suppressed wave component. This has been observed in side-heated shallow annular pools with thermally insulated bottom [20] shown in Fig. 11. We can call these HTWs near thermal boundary layers "degenerated" or "frustrated" HTWs because one wave component – the one in the direction of the applied temperature difference – does not develop; the degenerated HTWs travel parallel to the heated or cooled wall.

HTWs are as well degenerated if the gap between the hot and the cold wall is smaller than their wavelength component in this direction. In this case they travel azimuthally in annular gaps or cross the temperature gradient in channels because of this geometric restriction [21-22]. Stationary rolls have been observed in these so-called channels (Fig. 12) at larger depth d (e.g. $d > 3$ mm) [22] with the roll axis parallel to the applied temperature gradient (wave vector perpendicular to the applied horizontal temperature gradient). These stationary rolls (SR) could be related to the "linear rolls" of Smith and Davis [13]. Buoyancy might be the reason for these stationary rolls though thermocapillarity is dominating (to be discussed later). On the one hand the SRs have not been observed under microgravity for $2.5 \text{ mm} \leq d \leq 20$ mm, indicating that gravity is essential. On the other hand these 3D stationary rolls have been observed down to $d = 3$ mm, that is, at small gravity influence [23]. The increase of the flow amplitude of these stationary rolls indicates that the transition from the basic state to the roll state is not a Hopf bifurcation [23].A bifurcation of 2D buoyant thermocapillary convections to 3D (like SR) is indicated in numerical calculations [24].

Liquid bridges (LBs) constitute a special rotationally symmetric gap. The free surface is parallel to the gravity direction, the LBs must be short because of gravity and, the HTWs travelling in azimuthal direction must obey the periodic boundary condition $2 \pi a = m \cdot \lambda$ with a = LB-radius, λ = wavelength of the HTWs and m an integer. The temperature – and flow oscillations in the LBs have been investigated long before the studies of the related annular gaps [25].

It was found that the transition from steady flow to oscillatory flow (that is degenerated HTWs) is a Hopf bifurcation (Fig. 13) [25]. In a microgravity experiment on an extremely long LB (A = L/a = 15) the degeneration of the HTW was very effectively removed and a large axial wave component was observed besides the azimuthal one [26]. And it was found that the transition from the basic thermocapillary flow with return flow in the LBs is a Hopf bifurcation [24] (Fig. 14) [25].

The advantage of the confined very large temperature gradient near a heated or cooled metal wall seems to be the possibility to observe the so called "surface waves" predicted by Smith and Davis [27]. Thermocapillary surface waves (SWs) have been observed until now only in such thermal boundary layers [20, 28, 29] at the heated wall. SWs are due to a shear mechanism which is largest at the hot side in the boundary layer with the highest surface flow velocities. The dynamic deformation of the free surface is crucial for this instability whereas HTWs are found by linear stability analysis for nondeformable free surface. Fig. 15 shows a shadowgraphic image of free surface of an annular gap heated from the inner cylinder (r_i = 20 mm) and cooled from the outside container (r_o = 40 mm) and cooled from the outside container (r_o = 40 mm) with insulating bottom. The SWs in Fig. 15 travel from "hot" to "cold" and azimuthally.

Hydrothermal waves (HTWs) [13, 14], surface waves (SWs) [27], stationary rolls or linear rolls (SRs, LRs) [13, 22] and multicells (MCs) [30, 20, 14] (MCs see Fig. 16) have now been observed most likely in many configurations with different aspect ratios and thermal boundary conditions, but it is not easy to tell which case was observed and to compare the different works. In some experiments submerged heaters have been used [31-35] or the free surface was heated locally from above [36]. The temperature gradient along the free surface can be prescribed as linear like in the theoretical paper [13, 14] but can be supplied by heated/cooled walls with thermal boundary layers like in liquid bridges [25] and annular gap [16] but can as well be provided as a gradient in the conducting bottom [30]. Depending on the thermal conductivity of the bottom (glass [15, 22, 37, 38], quartz glass [23] or metal [30, 39]. The thermal boundary condition at the bottom can have a large influence on the type and threshold of the various thermocapillary instabilities. As well the degree of confinement (channel [30, 22] or LB [25, 40] with strong confinement or more extended layers or LBs [14, 15, 37, 26]) make a difference for the appearance of the instabilities. Interesting is as well the case where the "bottom" is made up by a large or a practically infinite vessel with thermocapillary acting on top, only [33, 35]. The influence of the thermal boundary conditions on the stability of thermocapillary flow is reviewed only for small Pr in [41] and a short review on experiments on thermocapillary instabilities can be found in [42].

2 Systems with higher complexity

2.1 Adding buoyancy to thermocapillarity

We consider an increasing depth d of the liquid with thermocapillarity driven in its horizontal free upper surface with extension L. Besides an increase of Ra as well A = L/d will approach a larger value

in most experiments. The experimental systems studied are either rectangular [22, 30, 37, 43-48] or circular, e.g. crucibles or annular gaps (to be discussed later).

In rectangular geometry we have influence of the sidewall, modulating the travelling direction of the HTWs [22, 30] or by inducing 3-D flow [43-48]. It was found that an increasing influence of buoyancy – e.g. by increasing d – will stabilize the flow against transition to time dependence [30]. Smaller critical Marangoni numbers have been found in experiments with annular gaps under microgravity compared with those under normal gravity [16, 50]. The influence of gravity on the Ma^c for the occurrence of HTWs is shown in Fig. 17. Increasing Bo(h) means increase of d. Gravity stabilizes the basic flow with multirolls against the transition to HTWs.

The 3D-stationary instability of longitudinal rolls found at larger d [22, 23, 37, 47] was not found under microgravity, indicating that it needs gravity influence to develop [16].

At larger d, e.g. d > 10 mm, the convection roll driven by thermocapillarity and buoyancy can separate from buoyancy driven convection in the bulk fluid [43-46]. This type of flow seems to be steady in contrast to that for d ≤ 3 mm which is time-dependent at comparably smaller Ma. The separation has been successfully simulated numerically by use of a rather fine mesh and by introducing temperature-dependent viscosity [49]. Moreover, one has to resolve the buoyant flow in the thermal boundary layers at both end walls and their connection with the thermocapillary flow to get a correct numerical simulation of the strength of the latter. Hotter liquid is circulating on top of colder liquid in the bulk in this separation of surface flow and its return flow from the bulk [43, 46, 49]. This separation of a thermocapillary convection roll (or layer) on top of the fluid is demonstrated in Fig. 18 by streaklines in a vertical light sheet and by holographic interferometry indicating the isotherms. It was as well observed in crucibles [50, 51] and its instability will be considered later when the separated "basic thermocapillary flow" is strongly cooled from above.

Turning from rectangular cavities to rotationally symmetric annular gaps or cylindrical vessels (crucibles with cooled or heated centres) does not change the nature of the HTWs or linear rolls. The advantage of this kind of geometry compared to the rectangular are avoidance of one pair of (inactive) sidewalls which could become disturbing due to extra lateral temperature gradients or by reflecting travelling HTWs. We mention work on annular gaps with not too large d [15, 16, 18] annular gaps with A up to A = 1 [33, 34, 16, 52] and crucible-like configurations [51]. For large A and small d HTWs are observed [15, 16] which form Archimedian spirals in this configuration because of an angle of approximately 45° between the wavevector and the temperature gradient (Fig. 6). The HTWs for the fluid with 7 ≤ Pr ≤ 17 have the travelling direction from "cold" to "hot." For smaller A some wavetrains are observed to travel mainly azimuthally [16, 33, 34, 52]. In a crucible with real Czochralski crystal growth configuration HTWs have been observed to travel azimuthally in the meniscus at the cooled crystal dummy [19]. Numerical simulation of Czochralski-growth systems of and oxide melt [53, 54] revealed azimuthally travelling waves as those observed in the model systems of annular gaps. But from real growth systems these HTWs have not yet been reported.

2.2 Temperature gradients inclined to the free surface

The motivation to study this problem is application; we encounter at the same time heating from the side and cooling from the top in many practical situations (e.g. in material processing like crystal growth from the melt after the Czochralski-technique). The possibility of an instability of thermocapillary flow in form of the classical Bénard-Marangoni instability by cooling from above is given. Indeed, small convection cells can be observed on the surface of high temperature melts to drift from "hot" places to "colder" ones (Fig. 19). The small wavelength λ of this cellular instability at the surface of oxide melt of considerable depth d ($2\lambda << d$) indicates the instability of a thin layer of the melt, only. We have seen in the preceding chapter that a time-independent surface roll can separate from the flow in the bulk (Fig. 20). We can take the flow profile of this separated surface tension convection as basic state for a new state when cooling from above. Two flow profiles can be studied

- separated flow with return flow
- linear flow (only from hot to cold without return flow) because the return flow is deeper in the bulk

Given a melting temperature of the order of 1800° C and a semitransparent melt (or even a black melt), the surface will be cooled very effectively by radiation. This can induce Bénard-Marangoni cells which will increase the heat transfer from the bulk to the free surface and through the free surface. Thus the heat flux through the free surface is enhanced what will turn increase the convective strength of the thermocapillary motion and the tendency for the above discussed separation. One can assume a Nusselt number Nu for the Bénard-Marangoni instability well above Nu = 2 because the value Nu = 1.8 has been reported for $Ma = 4 \cdot Ma^c$ from an experiment under microgravity [12]. Only for the correct simulation of the heat transport through the free surface and through the crystal. can one expect the correct simulation of buoyant-thermocapillary convection in the whole melt in the crucible. This, in turn, is needed to simulate the correct balance between buoyancy – thermocapillary convection and forced convection driven by crystal rotation which is decisive to simulate the crystal radius and the shape of the crystal-melt interface [56-58]. The basic ideas are sketched in Fig. 21. The flow – and temperature profile at the melt surface that can become instable due to cooling from above can be more a linear velocity profile (Figs. 21a, 4) or one with return flow (Fig. 21b). The type of drifting cells and their drift speed, the type of instability will be different for the two velocity profiles.

The stability of thermocapillary flow (with return flow) with inclined temperature gradient was investigated theoretically (Fig. 22) [59]. Transition to HTWs, transverse travelling rolls (TTRs) or square drifting cells and stationary lingitudinal rolls (LRs) are observed, depending on Ma_h and Ma_v. HTWs are stabilized by cooling from above (line 3 in Fig. 22, increase of Ma_v/Ma_h) as well observed in [60, 61]. Stationary longitudinal rolls have been observed by many experimenters mentioned above at increased liquid d though the parameter Ma_v/Ma_h in Fig. 22 is meant for increasing ΔT_v, only (d was fixed in [59]). The stationary rolls are as well observed in the experiments and numerical analysis

changing d and $\Delta T_v/\Delta T_h$ [61]. Transverse travelling rolls (or square drifting cells) have been observed cooling thermocapillary flow (Pr = 10) from above in experiments with controlled ΔT_h and ΔT_v [62]. The scenario and tendencies of figure 22 seem to be correct and are found in Czochralski melt growth.

In the situation sketched in Fig. 21 (a) only the linear flow profile, like that of linear thermocapillary flow becomes instable to cooling from above. This has been investigated in the same apparatus used in [39] to study linear thermocapillary flow and its instabilities at larger Ma_h. Figure 23 shows the pattern of convection cells drifting in linear thermocapillary flow cooled from above. The drifting speed of the cells is proportional to that of the flow speed in the free surface and much larger thant the drifting speed of convection cells observed in thermocapillary flow with return flow (as sketched in Fig. 21 (b)) [63]. Figure 24 indicates the stability threshold in terms of Ma_v. The difference between the experiments [39, 63] and that of separated thermocapillary flow on the top of oxide melts in Czochralski growth are the undefined thermal- and flow boundary conditions at the lower border of the latter. But the physics should be the same.

2.3 Static and dynamic surface deformations

The heat transfer properties of a flat and that of a curved surface can differ significantly. One example is the meniscus of a liquid at a heated wall when the liquid is fully wetting the wall in comparison to a liquid with flat surface pinned to e.g. the upper rim of the vessel. Thermocapillarity will be of another nature (e.g. stronger in case of a thermal boundary layer at the wall) in the meniscus region. Spontaneous convection can occur in the vicinity of a liquid meniscus in case of solute transfer across the curved interface [64]. Heat transfer across the meniscus interface will change thermocapillary flow, too. Thermocapillary flow is largest near the hot crucible wall in Czochralski systems of oxide materials because of the thermal boundary layer and, in accordance with Fig. 22, stationary linear rolls (called "spokes pattern" in the crystal growth literature) are observed there. In the regions with smaller horizontal temperature gradient or stronger cooling from above the pattern of linear rolls transforms into transverse travelling rolls or travelling cells [65].

Liquid bridges LBs are hydrostatically deformed by gravity in laboratory experiments and their volume V can be less than ideal, e.g. $V/V_o < 1$ (underfilled or necked-in LB) or more than ideal ($V/V_0 > 1$) (bulging LB). The stability of thermocapillary flow can depend strongly on V/V_0 with maximum stability near $V/V_0 = 1$ [66-68] in terms of a Marangoni number $Ma^* = |\partial\sigma/\partial T|\cdot\Delta T\cdot R\cdot\eta^{-1}\cdot\chi^{-1}$, with the temperature difference ΔT between the support rods and radius R of the LB. We note that most of the ΔT applied to the support rods is dropping in the thermal boundary layers on both end walls in the LB with Pr >> 1 investigated until now. Thus the meniscus-shape in a necked-in LB will provide a relatively better "thermal coupling" of the necked-in LB to the end walls than that provided for an ideal LB. The smaller Ma* for necked-in LBs is understandable, therefore. Heat transfer to the surrounding air can play a role for the critical Ma as well because buoyancy-driven convective rolls

together with thermocapillary-driven rolls are alive in the gas-surrounding of the LBs in normal experiments.

Known since Bénards experiments and measurements [9, 1] is the depression of the free surface at the spots of the hexagonal convection pattern where the hot fluid is rising. This hotter fluid has smaller surface tension which generates the depression. Thus it is principally impossible to investigate thermocapillary flow or Marangoni effects in liquids with a mirror-like flat surface. It is possible to prepare such a mirror-like flat free surface without meniscus at the wall of the vessel if no temperature gradients are applied. But a surface depression will be observed as soon as a wall is heated. The surface depression in its vicinity occurs because of uprising hot flow [20]. Time-independent flow and temperature gradients will deform the free surface statically and time-dependent states will generate time-dependent surface deformations. The dynamic surface deformations can be essential for the instability mechanism of thermocapillary flow or they can be only reactions to the flow instability.

The HTW in dynamic thermocapillary layers [13] have been derived in a stability analysis of layers with undeformable free surface and their properties compare well with HTWs observed in experiments [14, 15]. We conclude that the surface deformations observed in connection with the occurrence of HTWs are only reactions of the free surface to time-dependent flow. The same is true for the degenerated HTWs in liquid bridges; here experiments and numerical simulations of LBs with undeformable free surface show satisfactory agreement. As well the HTWs observed at the heated cylindrical inner wall of an annular gap [20] and those in the meniscus of a cooled dummy crystal in a Czochralski configuration [19] are small and of secondary importance for the occurrence of this instability.

An interesting case of surface oscillations was observed in the meniscus at a cold wall when – and only when – this meniscus had a certain height h and was pinned to the upper rim of this wall [29]. The experiments have been performed in a rectangular cavity of A = 1 (e.g. L = 20 mm, d = 20 mm, w = 41 mm) filled with ethanol (Pr = 17) with not to much underfilling below the normal volume V_0 = 20 x 20 x 41 mm^3 such that the menisci at all walls were still pinned to the upper rim. Macroscopic standing gravity-surface waves with amplitudes up to 0.5 mm have been excited in the surface of the liquid due to resonance with oscillations in the meniscus at the cold wall. The macroscopic gravity surface wave disappeared when the meniscus at the cold wall was no longer pinned but able to slide at the cold wall. It was concluded that the meniscus at the cold wall became instable to oscillations of the type of surface waves [27]. The frequency spectrum of these surface waves was tracked as spectrum of temperature oscillations in the meniscus and some peaks of this spectrum are found to be near the frequency peaks of gravity surface waves in this cavity. Tuning these frequency peaks of the gravity surface waves, by changing e.g. L, the resonance could be reinforced or suppressed (e.g. with L = 12 mm instead of L = 20 mm). Fig. 25 shows the amplitude of the standing wave in direction of the applied temperature gradient $\Delta T/L$ as function of the underfilling h (h measured from the top rim of the cavity) for a fixed ΔT = 27.5 K. The onset of the surface gravity waves is for h = 0.8 mm, and for

$\Delta T^c \sim 11.5$ K for h ~ 1.5 mm with frequencies of ~ 7 Hz (depending on mode and h). It was concluded that time-dependent flow in the meniscus is exiting the standing gravity waves (Fig. 26). The resonance is possible if the frequencies of the exiting and the exited oscillations are not too far apart and if at least one has a large enough half width in frequency (Fig. 27). We have here an example of the excitation of macroscopic standing gravity waves by small amplitude surface oscillations by oscillatory thermocapillary flow in case of resonance.

3 Systems of technical relevance

3.1 Solutocapillarity and dirt films

We will give some examples of thermocapillary flow or solutocapillary flow in systems of technical relevance. We leave the model substance "silicone oil" and turn to metals or crystal growth melts.

The surface tension and its temperature dependence are normally changed by impurities. Solutocapillary effects are often much stronger than thermocapillarity. Moreover, many liquids contain impurities which are surface active; e.g. these impurities can accumulate in the free surface as a film. Such a film can suppress thermocapillarity totally [44]. Water and mercury are examples of such liquids. Thermocapillarity and its instabilities can be studied reliably only in liquid systems without such surface films. Either high purity or very low surface tension of the liquid are used to reach this goal. Only a few liquids with higher surface tension seem to make no problems (e.g. $NaNO_3$-melt). If the surface is only partly covered by an impurity film, this film will be concentrated at the cold side and will be deformed by surface pressure of the flow [35] or the flow direction is changed [69]. A flow-reversal is known from arc welding where sulphur-impurities are known to produce this and the depth of the weld-bed can increase significantly by this flow reversal (from "cold" to "hot" in the free surface).

The surface tension of oxides is normally significantly smaller than that of the pure metal and solutocapillary effects can override thermocapillary ones. One example is given by a liquid Sn-droplet covered with a SnO_2-skin in high vacuum, bombarded with an ion beam on one spot [70]. It was sufficient to bombard only this spot to remove the whole SnO_2-skin because solutocapillarity is driving any SnO_2-skin towards the (heated) bombarded spot with its higher surface tension where the SnO_2 is sputtered away. Strong solutocapillary flow and flow instabilities including surface vibration have been observed in melt pools of Cu or of Sn blowing locally oxygen onto the melt surface [71].

The experiments to study the onset of oscillatory thermocapillary flow in LBs from mercury suffered under the presence of amalgame films [72] whereas careful the experiments on LBs from tin in high vacuum and with a getter (Ti at 600° C) to reduce the oxygen partial pressure yielded reliable results of Ma^c and the frequency [73]. The same is true for the studies of the instability of thermocapillary flow in LBs from silicon melt [74-75] or that in melt pools like in Czochralski crystal growth [76]. Many attempts to measure Ma^c in silicon melt have been undertaken because of the

technological importance of this material. It is not easy to compare the measurements and to predict the flow-state in industrial systems because of the high solubility of oxygen in Si-melts and the volatility of SiO at the melting temperature of Si; the surface tension of Si-melt shows a strong dependence on the oxygen partial pressure [77, 78] and the systems are not easily characterized.

We have the impression that experiments on "easy" model systems with liquids of high Pr are rather reliable because they can be characterized well enough and the physical parameters are known. Fundamental aspects of thermocapillary instabilities can be studied especially if the liquids are transparent. The critical Marangoni numbers measured at LBs from high Pr-liquids are rather reliable [79] and the extrapolation of the data to smaller Pr was successful. Figure 28 shows the measured critical Marangoni numbers in LBs with different Pr in comparison to theory for infinitely extended liquid layers.Only the tendency over Pr is satisfacory.

3.2 Thermocapillarity and solutocapillarity in interaction with moving crystal boundaries

Crystal growth is a nonequilibrium process. In melt growth we have the temperature gradient in front of the crystal-melt interface as the driving potential for the advancement of the solid interface. Thus we expect thermocapillary flow towards the crystal grown from the melt with free surface (floating zone technique, Czochralski technique). This flow transports heat towards the crystal. On the other hand the melt is never pure or it is even doped deliberately and impurities or dopants are not incorporated into the crystal as the main constituent. The dopants or impurities are normally enriched in the residual melt and the crystal is more pure than the melt. Defining the concentration of an impurity in the melt as c_m and that in the crystal grown with growth speed v as $c_s(v)$ we can define the segregation coefficient or distribution coefficient $k(v) = c_s(v)/c_m$. The effective distribution coefficient k(v) is smaller unity if the crystal contains less impurity and this impurity is enriched in front of the crystal growing with speed v in this case. We note that the impurity source is ceasing for zero growth speed. The impurity source provided by the growing crystal ceases as well for $v \to \infty$ because then $k(v) \to k(\infty) = 1$. The strength of the impurity source provided by a growing crystal is limited, therefore. We have thus the possibility to use the growing crystal as a source of rejected impurities and, if the impurity is e.g. lowering the surface tension, solutocapillary forces can drive flow in the free surface away from the growing crystal.

Different cases can arise

a) time-dependent thermocapillarity modulates the growth speed of the crystal and thus the amount of incorporated impurity.
b) solutocapillarity and thermocapillarity are directed parallel and reinforce each other
c) solutocapillarity is antiparallel to thermocapillarity and is weaking it
d) solutocapillarity is strong and counteracting thermocapillarity. New instabilities are possible.
e) the solute is surface-active, forming a film at the free surface, but partly soluble with solutocapillarity counter thermocapillarity. New instabilities are possible.

f) thermocapillary flow and forced flow by crystal rotation are counteracting and both are shaping the crystal interface, but differently, where the rotational action depends on the crystal shape. Instable situations for the flow and the interface are possible.

Some of these cases have been treated or observed.

a) A floating zone of Si-melt doped with Sb was crystallized under microgravity from one side with 1 mm/min and the temperature oscillations by time-dependent thermocapillary flow have been measured together with growth rate oscillations [80]. From the good correspondence of both signals it was concluded that the growth speed of the crystal was reacting on the flow - and temperature - oscillations of thermocapillary flow. A quite similar result was obtained by other authors in laboratory experiments [78].

c)-d) A thin sheet Bi-crystal was grown by dircetional solidification. at high growth velocities v from a Sn-0.11 at % Bi melt-layer of 2 mm thickness with free surface under a temperature gradient of approximately 10 K/cm. The authors could observe a coordinated back and forth motion of the meniscus line [81]. For the doping of Sn with Bi a flow reversal is observed for some concentrations (e.g. $c < 0.5$ at % Bi) and solutocapillary flow can oppose thermocapillary one. This work seems to be an example of the active involvement of the growing crystal into the thermocapillary-solutocapillary instability.

d)-e) This active participation of the crystal in the instability has been observed in LBs from $NaNO_3$ faintly doped with the surface-active impurity CH_3CH_2COOK and recrystallized from below [82]. The surface tension of $NaNO_3$ is lowered dramatically by the impurity and the impurity is rejected by the crystal. We thus have solutocapillarity opposing thermocapillarity. In contrast to the well-known passive growth oscillations discussed above under a) [78, 80] the growth and remelting of the crystal is taking part acitvely in this instability. The full mechanism of this new type of instability is outlined in this paper [82]. We outline one part of the instability-cycle: The crystal is a source of impurity, increasing solutocapillarity during growth. This decreases the convective heat transport to the crystal because thermocapillarity is consequently weakened. The convective heat transport to the crystal is weakened. Thus the growth speed is increasing more and more. This is limited by the applied temperature gradient and by $k \rightarrow 1$. The reverse happens once remelting starts because pure substance is remelted, weakening solutocapillarity (strengthening thermocapillarity). The impurity CH_3CH_2COOK might form a film on $NaNO_3$-melt.

Solutocapillarity as analogue to thermocapillarity in a LB was studied numerically [83]. The source for the solute gradient was the growing crystal and the solute distribution differs from the temperature distribution for thermocapillarity, therefore. For certain conditions the authors found a Hopf bifurcation from the basic flow to HTWs.

A dramatic interaction between buoyant-thermocapillary flow and forced flow by crystal rotation was observed in Czochralski growth of high melting point oxides [58]. The crystal has a strong conical interface deflection during the beginning of growth because of large radiative heat transport through it. The rotationally driven convection roll has a smaller strength near the free melt surface for a conical interface than for a flat interface. The rotation of the crystal is chosen by the crystal grower in a way that the balancing point (stagnation point) between forced convection and buoyant-thermocapillary convection is near the crystal periphery to controll the crystal radius. This situation is instable during the increase of the crystal radius (Fig. 29) because of the following reaction chain: a small increase in crystal radius r at a certain crystal radius will increase rotationally driven convection. This in turn will melt-back a part of the crystal cone below the surface and this increases the strength of rotational convection near the interface. The stagnation point is shifted outwards because of this and the convective heat transport towards the crystal by thermocapillarity is weakened, resulting in further increase of the crystal radius. Thus the crystal radius will increase uncontrollable and the flow near the crystal interface changes from "buoyant-thermocapillary dominated" to "rotationally dominated." The reason for the significance of thermocapillary convection in this flow transition is the fact that both, thermocapillarity and forced convection by a flat rotating crystal interface are acting and balancing near the free melt surface whereas radial outwards convection by a rotating conical interface below the surface is stronger in the bulk of the melt and not in the interface.

4 Conclusions

Thermocapillary convection with its instabilities and effects in melt processing (mainly crystal growth from the melt) has been reviewed from an experimental point of view. We propose to interpret the thermocapillary instabilities observed in the more complex systems as derivable from the instabilities found in the model systems, like hydrothermal waves or linear rolls or Bénard cells in infinitely extended layers. We found tendencies supporting this view although the conclusion is not unambiguous.

The presented material covers mainly liquids with $Pr > 1$. Metallic liquids with $Pr << 1$ are only touched and their larger difficulties with defined surface properties (e.g. oxide films) are pointed out.

The literature cited in the article can by no means be complete but can serve as a source to cover the complete field.

Crystal growth from the melt is an prospective area to apply the knowledge about thermocapillary (Marangoni) instabilities because of two reasons:

1. The melt adjacent to the growing crystal has a free surface in the Czochralski technique, in the floating zone technique and in directional solidification in horizontal geometry. The free surface is mandatory to avoid heterogeneous nucleation and is thus mandatory for the growth of perfect single crystals. All ingredients for thermocapillary flow and Marangoni instabilities are given.

2. Large temperature gradients near the growing crystal interface are mandatory to avoid constitutional supercooling with its catastrophic effect for crystal quality.

We thus have liquid systems in melt growth with all ingredients for strong thermocapillary flow and its instabilities. Moreover, the growing (moving) crystal interface can react to flow oscillations (heat transport fluctuations) and can incorporate them as dopant striations. Solutocapillary effects can be introduced by the segregation connected with crystallization. The crystal can even play an active rôle in thermocapillary – solutocapillary instabilities.

References

[1] Koschmieder E L 1993 *Bénard Cells and Taylor Vortices* (Cambridge: Univesity Press)

[2] Kuhlmann H C 1999 *Thermocapillary Convection in Models of Crystal Growth* (Berlin: Springer)

[3] *Interfacial Phenomena and Convection* 2002 Monographs and Surveys in Pure and Appl. Math Vo. 124 eds Nepomnyashchy A A, Velarde M G and Colinet P (CRC: Chapman & Hall)

[4] *Interfacial Phenomena and the Marangoni Effect* 2002 CISM Courses and Lectures No 428 eds Velarde M G and Zeytounian R Kk (Wien New York: Springer)

[5] *Interfacial Fluid Dynamics and Transport Processes* 2003 Lecture Notes in Physics eds Narayanan R and D Schwabe (Berlin: Springer)

[6] *Liquid Interfacial Systems*2003 Surface Science Series Vol 113 eds Birikh R V, Briskman V A, Velarde M G and J-C Legros (New York: Marcel Dekker)

[7] Schwabe D *Marangoni Effects in Crystal Growth Melts* 1981 *Physico Chemical Hydrodyn* **2** 263

[8] Schwabe D *Surface-Tension-Driven Flow in Crystal Growth Melts* 1988 *Crystals Growth, Properties, and Applications* Vol 11 ed Freyhardt HC (Berlin: Springer)

[9] Bénard H 1900 *Rev Gén Sci pure Appl* **11** 1261

[10] Pearson J R A 1958 *J Fluid Mech* **4** 489

[11] Nield D A 1964 *J Fluid Mech* **19** 341

[12] Schwabe D 2006 *Exp. Fluids DOI 10.1007/s00348-006-0130-0*

[13] Smith M K and Davis S H 1983 *J Fluid Mech* **132** 119

[14] Riley R and Neitzel G 1998 *J Fluid Mech* **359** 143

[15] Garnier N Chiffauded A 2001 *Eur Phys J B* **19** 87

[16] Schwabe D, Zebib A and Sim B-Ch 2003 *J Fluid Mech* **491** 239

[17] Sim B-Ch, Zebib A and Schwabe D 2003 *J Fluid Mech* **491** 259

[18] Busse F H, Pfister G and Schwabe D *Formation of dynamical structures in axisymmetric fluid systems* 1998 in *Evolution of Spontaneous Structures in Dissipative Continuous Systems* LN in physics m 55 eds Busse F H and Müller St Springer Berlin

[19] Hintz P *Konvektion im Czochralski-Tiegel* 1999 *Dissertation Universität Giessen*, Giessen, Germany

[20] Schwabe D, Möller U, Schneider J and Scharmann A 1992 *Phys Fluids A* **4** 2368

[21] Burguete J, Mukolobwiez N, Daviaud F, Garnier N and Chiffaudel A 2001 *Phys Fluids* **13** 2773

[22] Daviaud F and Vince J M 1993 *Phys Rev E* **48** 4432

[23] Benz S and Schwabe D 2001 *Exp Fluids* **31** 409

[24] Mundrane M and Zebib A 1993 *Phys Fluids A* **5** 810

[25] Preisser F, Schwabe D and Scharmann A 1983 *J Fluid Mech* **126** 545

[26] Schwabe D 2005 **Phys Fluids 17** 112104

[27] Smith M K and Davis S H 1983 *J Fluid Mech* **132** 145

[28] Schneider J, Schwabe D and Scharmann A 1996 *Experiments on surface waves in dynamic thermocapillary liquid layers* in: *Microgravity sci technol* **9** 86

[29] Bach Ch *Resonanz von Oberflächenwellen mit thermokapillaren Instabilitäten in einem Meniskus* 2000 *Dissertation Universiät Giesse Germany*

[30] Villers D and Platten J K 1992 J Fluid Mech **234** 487

[31] Vince J M and Dubois M 1992 *Europhys Lett* **20** 505

[32] Ezersky A B, Garcimartín A, Burguete J, Mancini H L and Pérez-García C 1993 *Phys Rev E* **47** 1126

[33] Kamotani Y, Lee J H, Ostrach S and Pline A 1992 *Phys Fluids A* **4** 955

[34] Kamotani Y, Ostrach S and Masud J 2000 *J Fluid Mech* **410** 211

[35] Mizev A.I. 2004 *Appl Mech Tech Physics* **45** 486

[36] Favre E and Blumenfeld L 1997 *Phys Fluids* **9** 1473

[37] Burguete J, Mukolobwiez N, Daviaud F, Garnier N and Chiffaudel A 2001 *Phys Fluids* **13** 2773

[38] De Saedeleer C, Garcimartin A, Chavepeyer G and Platten J K 1996 *Phys Fluids* **8** 670

[39] Ospennikov N A and Schwabe D 2004 *Exp Fluids* **36** 938

[40] Tagaya E, Ueno I and Kawamura H 2003 *Thermal Sci & Engineering* **11** 45

[41] Priede J and Gerbeth G 1997 *Phys Fluids* **9** 1621

[42] Schatz M F and Neitzel G P 2001 *Annu Rev Fluid Mech* **33** 93

[43] Schwabe D and Metzger J 1989 *J Crystal Growth* **97** 23

[44] Schwabe D and Scharmann A 1988 *Adv Space Res* **8** 175

[45] Metzger J *Raumzeitliche Strukturen reiner und mit Schwerkraft gekoppelter thermokapillarer Konvektion* 1994 *Dissertation University of Giessen*

[46] Schwabe D and Dürr H 1996 *Microgravity sci technol* **9** 201

[47] Gillon P and Homsy G M 1996 *Phys Fluids* **8** 2953

[48] Braunsfurth M G and Homsy G M 1997 *Phys Fluids* **9** 1277

[49] Bueckle U and Perić M 1992 *Num Heat Transfer A* **21** 121

[50] Schwabe D 2002 *J Crystal Growth* **237-239** 1849

[51] Hintz P, Schwabe D and Wilke H 2001 *J Crystal Growth* **222** 343

[52] Lavally R, Amberg G and Alfredsson H 2001 *Eur J Mech B* **20** 771

[53] Jing C J, Imaishi N, Yasuhiro S, Sato T and Miyazawa Y 2000 *Int J Heat Mass Transf* **43** 4347

[54] Jing C J, Imaishi N, Sato T and Miyazawa Y 2000 *J Crystal Growth* **216** 372

[55] Miller D C *The role of fluid flow phenomena in the Czochralski growth of oxides* 1982 in: *Materials processing in the reduced gravity environment of space Ed Rindone G E Elsevier*

[56] Derby J J and Xiao Q 1991 *J Crystal Growth* **113** 575

[57] Schwabe D, Sumathi R R and Wilke H 2003 *J Crystal Growth* **265** 440

[58] Schwabe D, Sumathi R R and Wilke H 2003 *J Crystal Growth* **265** 494

[59] Nepomnyashchy A A, Simanovskii I B and Braverman L M 2001 *J Fluid Mech* **442** 141

[60] Sim B-C, Zebib A and Schwabe D 2003 *J Fluid Mech* **491** 259

[61] Hoyas S, Mancho A M, Herrero H, Garnier N and Chiffaudel A 2005 *Phys Fluids* **17** 054104

[62] Mizev A I *private communication*

[63] Schwabe D, Mizev A I and Ospennikov N A 2007 *Exp Fluids to be published*

[64] Kayser W V and Berg J C 1971 *Ind Eng Chem Fundam* **10** 526

[65] Schwabe D *Marangonikonvektion in Schmelzen* 1981 *Habilitationsschrift University Giessen Germany*

[66] Hu W R, Shu J Z, Zhou R and Tang Z M 1994 *J Crystal Growth* **142** 379

[67] Shevtsova V M and Legros J-C 1998 *Phys Fluids* **10** 1621

[68] Sumner L B S, Neitzel G P, Fontaine J-P and Del'Aversana P 2001 *Phys Fluids* **13** 107

[69] Pride J, Cramer A, Bojarevics A, Gelfgat A Yu, Bar-Yospeh P Z, Yarin A L and Gerbeth G *Phys Fluids* **11** 3331

[70] Fine J, Hardy S C and Andreadis T D 1981 *J Vac Sci Technol* **18** 1310

[71] Brimacombe J K and Weinberg F 1972 *Metallurg Transact* **3** 2298

[72] Han J H, Sun Z W, Dai L R, Xie J C and Hu W R 1996 *J Crystal Growth* **169** 129

[73] Yang Y K and Kou S 2001 *J Crystal Growth* **222** 135

[74] Croell A, Mueller-Sebert W and Nitsche R 1989 *Mat Res Bull* **24** 995

[75] Nakamura S, Hibiya T, Kakimoto K, Imaishi I, Nishizawa S, Hirata A, Mukai K, Yoda S and Morita T J 1998 *J Crystal Growth* **186** 402

[76] Hibiya T, Nakamura S, Sumiji M and Azami T 2002 *J Crystal Growth* **237** 1854

[77] Hibiya T, Nakamura S, Mukai K, Niu Z, Imaishi N, Nishizawa S, Yoda S and Koyama M 1998 *Phil Trans R Soc Lond A* **356** 899

[78] Sumiji M, Nakamura S, Azani T and Hibiya T 2001 *J Crystal Growth* **223** 503

[79] Velten R, Schwabe D and Scharmann A 1991 *Phys Fluids A* **3** 267

[80] Schweizer M, Croell A, Dold P, Kaiser Th, Lichtensteiger M and Benz K W 1999 *J Crystal Growth* **203** 500

[81] Camel D, Tison P and Tosello I *Solutal capillary convection during directional solidification of Sn-Bi liquid layers* 1994 *Proc Int Conf High Temperature Capillarity*, Smolenic Castle Ed Eustathopoulos, Reproprint Bratislava

[82] Schwabe D, Da X and Scharmann A 1996 *J Crystal Growth* **166** 483

[83] Witkowski L M and Walker J S 2002 *Phys Fluids* **14** 2647

Figure captions

Fig. 1. Hexagonal convection pattern in a liquid layer heated from below and cooled from above, visualized by a Shadowgraph technique [1].

Fig. 2. Stability diagram for the Bénard-Marangoni-Instability including the action of gravity [11].

Fig. 3. Convection pattern of the pure Marangoni-Instability in a small circular layer with free upper surface under microgravity (A = D/d = 5, Ma = 7 Ma^c). Visualization with fine aluminum flakes. The up- and down-flow regions are dark [12].

Fig. 4. Basic state flow profiles of dynamic thermocapillary layers. A temperature gradient in the free surface or a temperature difference between the walls drives this flow.
(a) linear flow profile of thermocapillary flow (without return flow)
(b) thermocapillary flow with return flow
These flow profiles can be modified by the action of gravity.

Fig. 5. Hydrothermal waves in a layer from silicone oil with d = 1.0 mm, travelling under an angle of 24° between temperature gradient and wave vector from " cold " to " hot." (From "left" to "right"). Visualization with IR camera [14].

Fig. 6. Hydrothermal waves in an open annulus with small diameter inner cooled wall in form of an Archimedian spiral [15]. Shadowgraph technique (d = 1.9 mm, ΔT = 14.5 K, Pr = 10).

Fig. 7 Hydrothermal waves in an open annulus with d = 20 mm and A = 1 under microgravity (silicone oil, Pr = 6.8). An IR camera shows the temperature distribution at the free surface [16]
(a) five wavetrains at $Ma \approx 2 \cdot Ma^c$ travelling azimuthally (experimental)
(b) nearly chaotic at $Ma \approx 4 \cdot Ma^c$ (experimental)

Fig. 8. Simulated surface temperature distribution for the same annular gap as in Fig. 7 with Bi = 0 [17]
(a) slightly above Ma^c
(b) at approximately $3 \cdot Ma^c$
The five wavetrains (m = 5) rotate clockwise and m does not change when increasing Ma.

Fig. 9. Sketch of the Czochralski crystal growth technique and the thermocapillary open annulus investigated in [16, 17].

Fig. 10 HTWs in the meniscus at the cold dummy crystal (copper) with r = 4 mm, $\omega_{crystal}$ = 0 in a crucible with R = 20 mm, liquid height H = 30 mm, ΔT = 25 K. Observation under diffuse illumination through the crucible bottom [19].

Fig. 11. HTWs in a shallow liquid layer (Pr = 17) in an annular gap near the heated wall with the bottom of the gap cooled. The HTWs deform the free surface and this deformation can be visualized by surface reflection shadowgraphy. (L = 20 mm, d = 1.8 mm, ΔT = 34 K) [20]

Fig. 12. (a) Linear rolls by shadowgraphy. View through the channel-like layer (d = 6 mm, ΔT_x = 6 K, L_x = 30 mm, Pr = 10). The cold side is down, menisci at cold and hot side [37]

(b) Critical temperature differences for travelling waves (TW) = HTW and stationary rolls (SR) = LR in layers with different height h = d in a rectangular gap with glass bottom with L = 10 mm (Pr = 10)

Fig. 13. The amplitude of temperature oscillations in a liquid bridge heated from the top by ΔT with Pr = 8 above the threshold increase as $(\Delta T - \Delta T^c)^{0.6}$. The exponent 0.6 is near 0.5 of a Hopf bifurcation [25].

Fig. 14. Squared amplitude of the temperature oscillations in a LB with A = 15 under microgravity over the applied temperature difference ΔT indicating a Hopf bifurcation [25].

Fig. 15. Surface wave (SW) with m = 6 in a 20 mm wide annular gap heated from the inside cylinder with r_i = 20 mm (d = 3.1 mm, ΔT = 24 K). The free surface in the gap is prepared as totally flat (no menisci at both sides) to allow shadowgraphy of light reflected from the free surface to visualize the SWs [28].

Fig. 16. Streamlines of multicellular (steady) thermocapillary convection in Pr = 4 fluid heated from the right-side. The cell axes are perpendicular to the temperature gradient. For larger Ma HTWs can travel from "cold" to "hot" (or vice versa depending on Pr) and the multicells will oscillate according to the HTW frequency [30]. The multicellular state can serve as basic state for HTWs [14, 16].

Fig. 17. The critical Ma increases with Bo, that is for increasing d, because of increasing gravitational effects (planar HTWs in extended rectangular cavities) [37].

Fig. 18. (a) Streaklines and (b) isotherms by holographic interferometry in a cubic fluid cavity with L = H = 20 mm at ΔT = 4 K (Pr = 17). The cavity has a flat free surface without any menisci at its side walls [46]. Indicated is the separation of a thermocapillary convection roll with hot fluid on top of cold fluid in the bulk.

Fig. 19. Cellular convection pattern observed on Garnet melt surface (melting point ~ 1750° C) with a melt depth d > 30 mm, drifting rapidly radially inwards to the coldest spot of the surface. Note linear rolls (steady) near the heated wall also called "spokes", note cross cells between the spokes (drifting) and chaotic Bénard-like cells in the centre [55].

Fig. 20. Streaklines in a 40 mm ∅ crucible, liquid depth d = 20 mm, different ΔT between hot crucible and cold crystal dummy, showing the separation of the surface tension driven convection from bulk convection [51].

Fig. 21. The counterbalance of buoyant-thermocapillary and rotationally driven flow in a high-temperature melt (Pr >> 1). A thermocapillary-driven flow can separate from the bulk flow, balancing the rotational one. And this "linear" flow profile (a) can become instable (to Bénard-like convection cells) due to large radiative heat loss from the melt surface. This heat loss is largest near the centre of the crucible or near the crystal. The instability in form of rolls or cells can reach down to the return flow (b) if the return flow is very near the surface flow due to strong separation.

Fig. 22. Stability diagram of thermocapillary flow with inclined temperature gradient, expressed by the relation between the vertical Marangoni number Ma_v and the horizontal one, Ma_h. The line "H-F" marks the transition to oblique hydrothermal waves, line "F-E" that to transverse travelling rolls and lines 1 and 2 that to stationary longitudinal rolls [59].above the threshold

Fig. 23. Linear thermocapillary flow without return flow cooled from above (sapphire lid with temperature gradient parallel to that in the metal bottom) shows convection cells drifting with the linear flow for Ma_v above the threshold. Visualization with IR camera, IR illumination and aluminum flakes. (d = 1.34 mm, Ma_v = 12.6, Ma_v = 132, Pr = 10) [63]. In the right part of the figure (hot) Ma_v is too small for the cellular instability and linear rolls can be observed.

Fig. 24. Stability limits of linear thermocapillary flow cooled from above [63]. For a certain Ma_h with linear flow we find with increasing Ma_v

- ○ stable linear flow
- ● longitudinal rolls
- ◊ transition from rolls to drifting cells (guessed)
- ▪ drifting cells

Fig. 25. The amplitude of standing surface gravity waves in a cavity with L = 20 mm, d = 20 mm, W = 41 mm, ΔT = 27.5 K when the underfilling h from a flat free surface is increased up to h = 1.4 mm. Onset at h = 0.8 mm [29].

Fig. 26. Spectra of hydrodynamic instabilities in the meniscus (red) and spectra of standing surface gravity waves in a cavity (L = 20 mm, W = 41 mm, ΔT = 25 K, underfilling h = 1.5 mm). The frequencies of the hydrodynamic instabilities (e.g. "a") are near to surface waves frequencies to excite these (e.g. mode k = 1, l = 1) [29].

Fig. 27. Time-dependent flow in the meniscus at the cold wall (L = 12 mm, W = 41 mm, ΔT = 45.5 K, h = 1.8 mm). The thermocapillary vortex fills only the upper part of the meniscus and secondary vortices are visible below it [29].

Fig.28. The measured critical Marangoni numbers in liquid bridges and layers (symbols) are generally larger than the theoretical ones (lines from[13]) but with the correct tendency. The reason for the discrepancy might be uncontrolled surface tension properties for the metallic systems (oxide impurities) and for the high-Pr liquids the “consumtion“ of the largest part of the applied temperature gradient in the thermal boundary layers. The critical value measured at liquid layers with temperature gradient in the metal bottom is nearest to theory, therefore.

Fig. 29. The counterbalance between buoyant-thermocapillary and rotationally driven flow of a flat interface (K/r = 0) and a conically deflected one (K/r = 1) (crystal radius r, stagnation point at r_s, rotational Reynolds number $Re = 2 \pi f r^2/\nu$).

a) Experimental result of the stagnation position for two different K/r at constant buoyant-thermocapillary flow; the flat interface needs smaller Re to shift the stagnation point to $r_s/r = 0.9$.
b) Numerical result on flow and stagnation positions (SP) for two interface shapes (flat on the left side, conical on the right side) for else unchanged boundary conditions for the flow.

Though the boundary conditions of the experiment are used for the simulation, the simulation does not show the separation of the thermocapillary flow observed in the experiments. The separation of

the thermocapillary flow could increase the observed difference in the action of a flat and a conical interface [58].

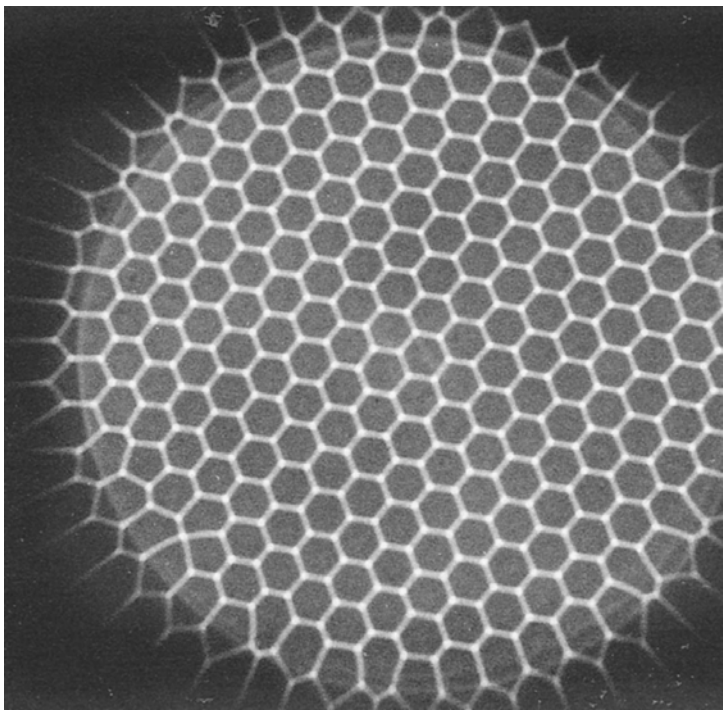

Fig. 1. Hexagonal convection pattern in a liquid layer heated from below and cooled from above, visualized by a Shadowgraph technique [1].

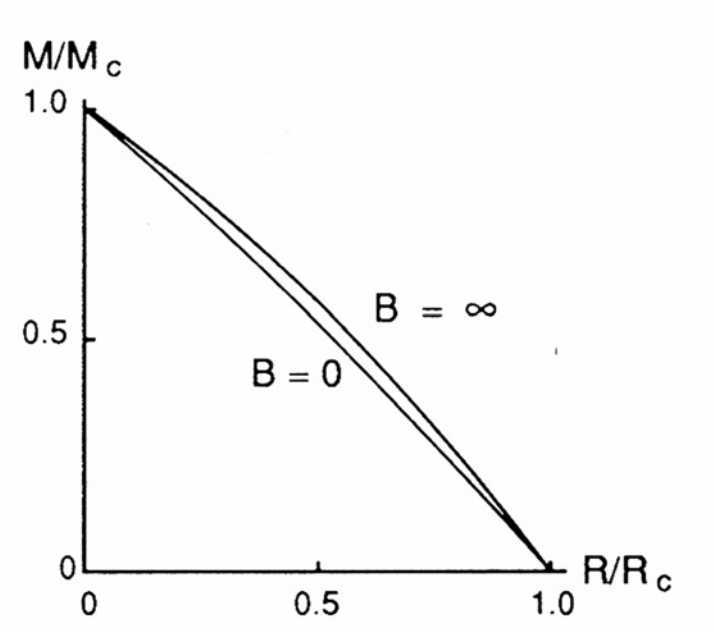

Fig. 2. Stability diagram for the Bénard-Marangoni-Instability including the action of gravity [11].

Fig. 3. Convection pattern of the pure Marangoni-Instability in a small circular layer with free upper surface under microgravity (A = D/d = 5, Ma = 7 Ma^c). Visualization with fine aluminum flakes. The up- and down-flow regions are dark [12].

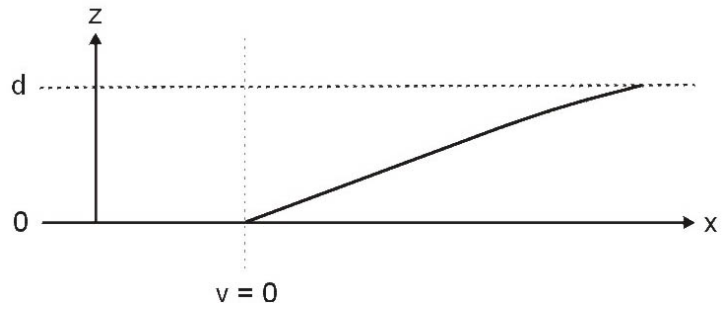

(a)

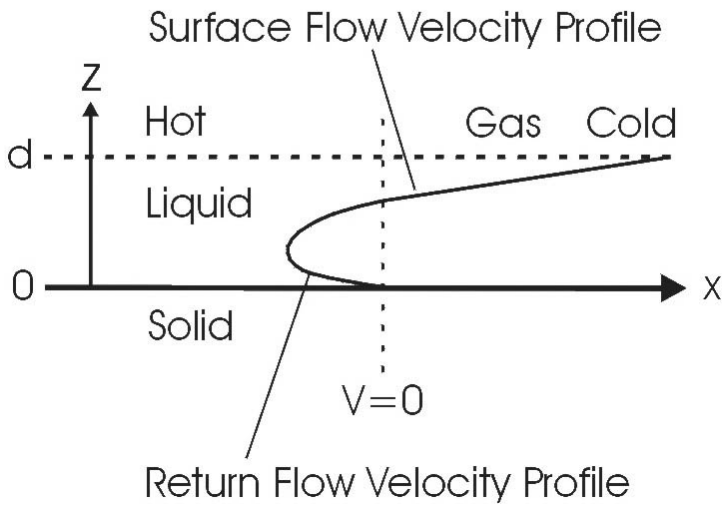

(b)

Fig. 4. Basic state flow profiles of dynamic thermocapillary layers. A temperature gradient in the free surface or a temperature difference between the walls drives this flow.
(a) linear flow profile of thermocapillary flow (without return flow)
(b) thermocapillary flow with return flow
These flow profiles can be modified by the action of gravity.

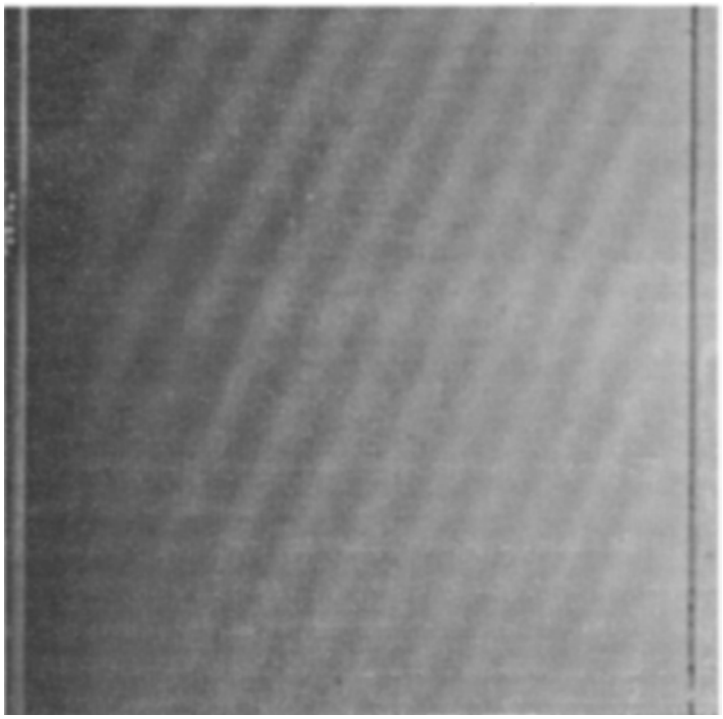

Fig. 5. Hydrothermal waves in a layer from silicone oil with d = 1.0 mm, travelling under an angle of 24° between temperature gradient and wave vector from " cold " to " hot." (From "left" to "right"). Visualization with IR camera [14].

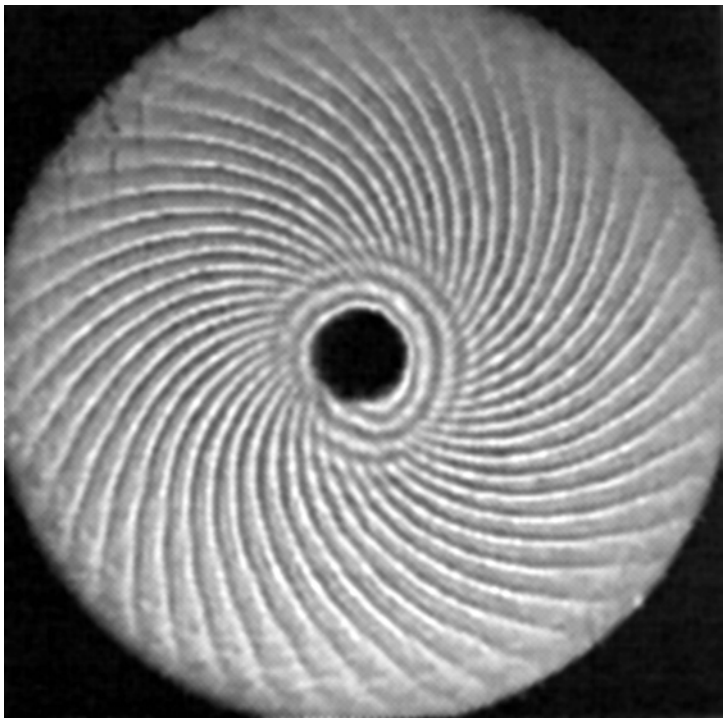

Fig. 6. Hydrothermal waves in an open annulus with small diameter inner cooled wall in form of an Archimedian spiral [15]. Shadowgraph technique (d = 1.9 mm, ΔT = 14.5 K, Pr = 10).

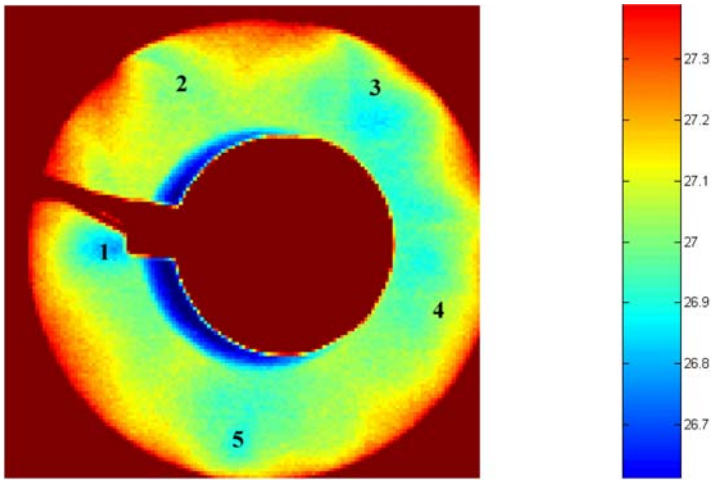

(a)

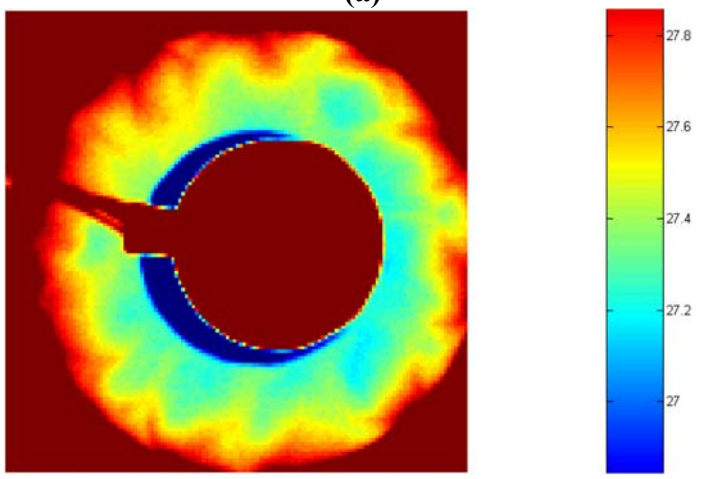

(b)

Fig. 7 Hydrothermal waves in an open annulus with d = 20 mm and A = 1 under microgravity (silicone oil, Pr = 6.8). An IR camera shows the temperature distribution at the free surface [16]
(a) five wavetrains at Ma ≈ 2 · Ma^c travelling azimuthally (experimental)
(b) nearly chaotic at Ma ≈ 4 · Ma^c (experimental)

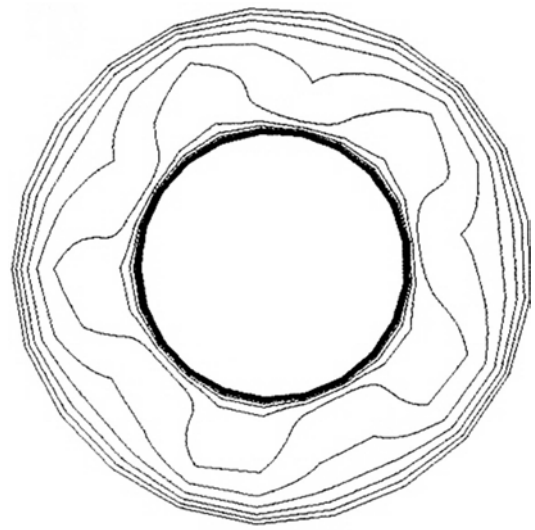

(a)

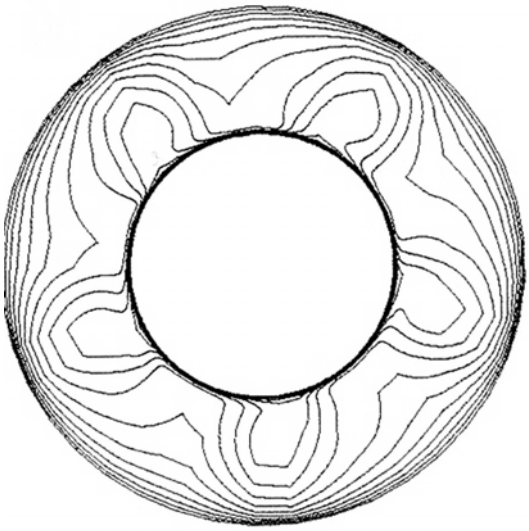

(b)

Fig. 8. Simulated surface temperature distribution for the same annular gap as in Fig. 7 with Bi = 0 [17]
(a) slightly above Ma^c
(b) at approximately $3 \cdot Ma^c$
The five wavetrains (m = 5) rotate clockwise and m does not change when increasing Ma.

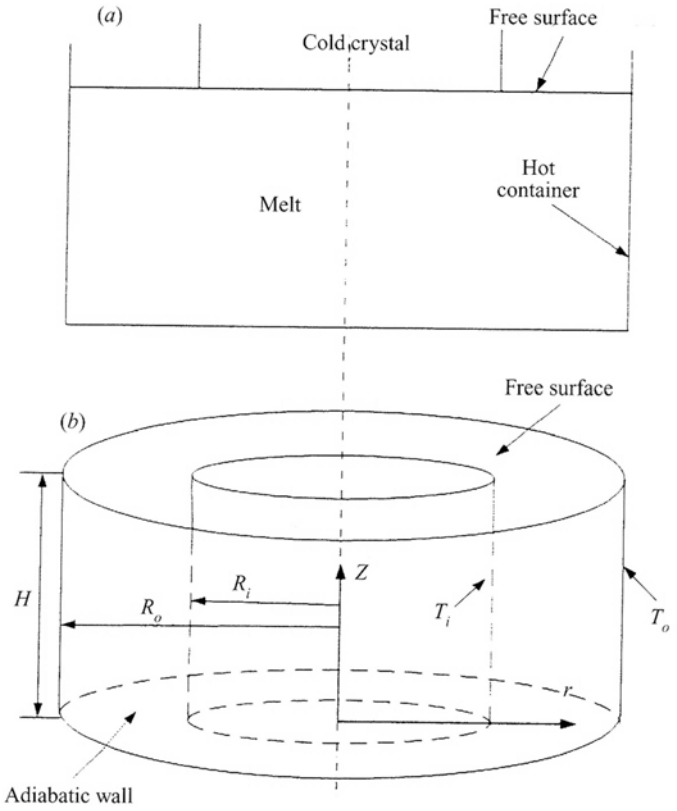

Fig. 9. Sketch of the Czochralski crystal growth technique and the thermocapillary open annulus investigated in [16, 17].

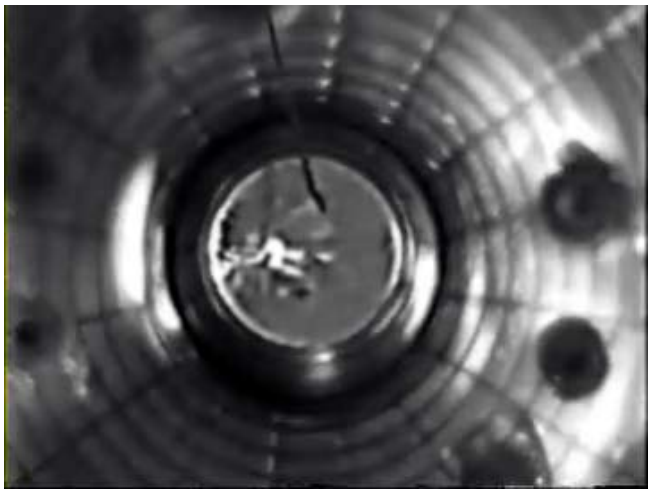

Fig. 10 HTWs in the meniscus at the cold dummy crystal (copper) with r = 4 mm, $\omega_{crystal} = 0$ in a crucible with R = 20 mm, liquid height H = 30 mm, ΔT = 25 K. Observation under diffuse illumination through the crucible bottom .The small inner grey circle is the face of the dummy seem from below.A thermocouple (black wire) comes from above and whithe schlieren (generated by the jet of cold liquid falling down from the cold dummy are visible on the grey dummy-face. The HTWs are visible in the video clip on the web page given in the abstract under "HTW in the meniscus"[19].

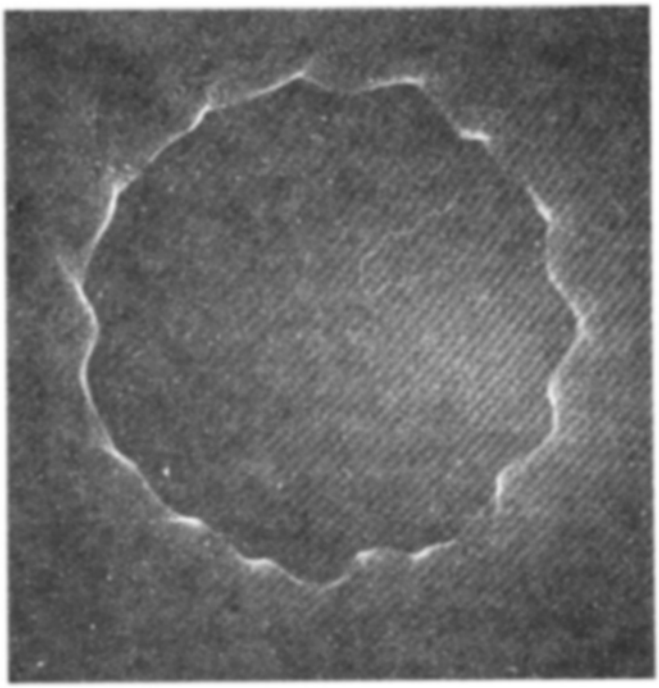

Fig. 11. HTWs in a shallow liquid layer (Pr = 17) in an annular gap near the heated wall with the bottom of the gap cooled. The HTWs deform the free surface and this deformation can be visualized by surface reflection shadowgraphy. (L = 20 mm, d = 1.8 mm, ΔT = 34 K) [20]

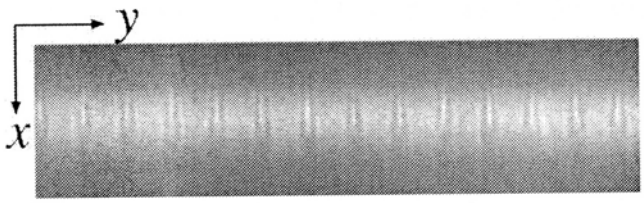

(a)

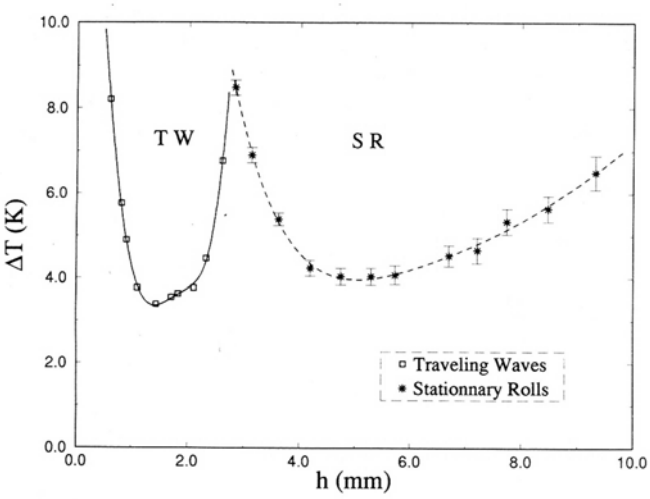

FIG. 3. Critical temperature difference ΔT_c vs the height of liquid h.

(b)

Fig. 12. (a) Linear rolls by shadowgraphy. View through the channel-like layer (d = 6 mm, ΔT_x = 6 K, L_x = 30 mm, Pr = 10). The cold side is down, menisci at cold and hot side [37]
(b) Critical temperature differences for travelling waves (TW) = HTW and stationary rolls (SR) = LR in layers with different height h = d in a rectangular gap with glass bottom with L = 10 mm (Pr = 10)

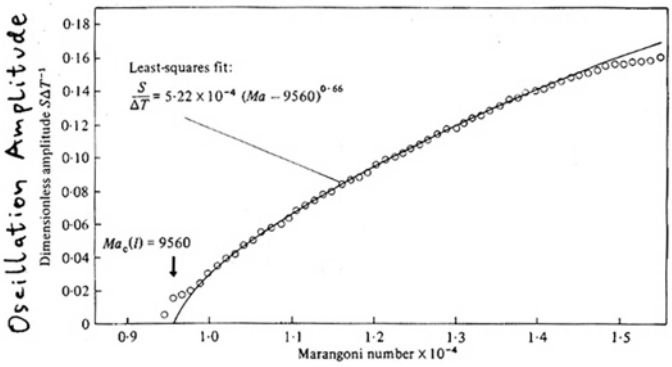

Fig. 13. The amplitude of temperature oscillations in a liquid bridge heated from the top by ΔT with Pr = 8 above the threshold increase as $(\Delta T - \Delta T^c)^{0.6}$. The exponent 0.6 is near 0.5 of a Hopf bifurcation [25].

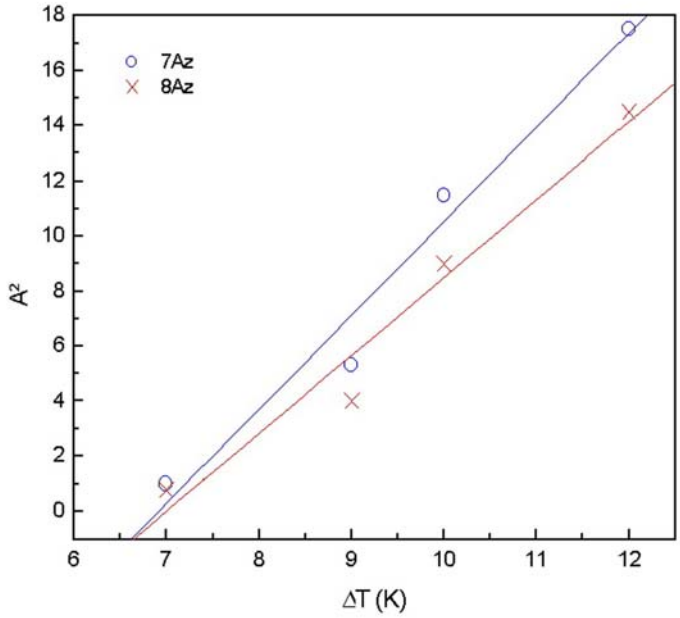

Fig. 14. Squared amplitude of the temperature oscillations in a LB with A = 15 under microgravity over the applied temperature difference ΔT indicating a Hopf bifurcation [25].

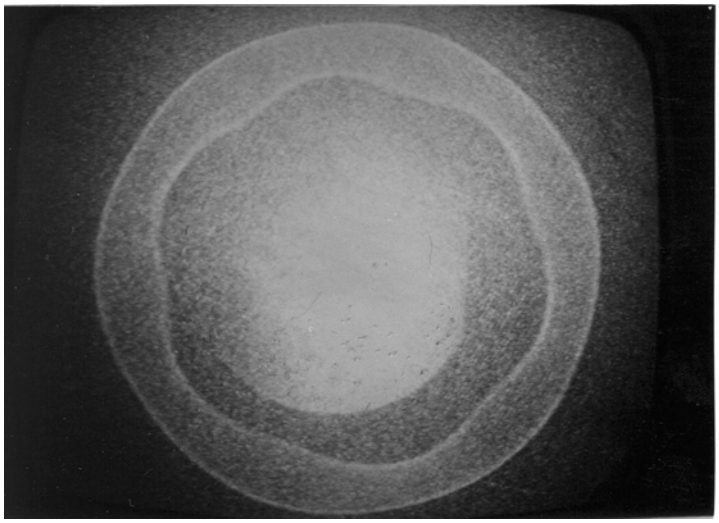

Fig. 15. Surface wave (SW) with m = 6 in a 20 mm wide annular gap heated from the inside cylinder with r_i = 20 mm (d = 3.1 mm, ΔT = 24 K). The free surface in the gap is prepared as totally flat (no menisci at both sides) to allow shadowgraphy of light reflected from the free surface to visualize the SWs [28].

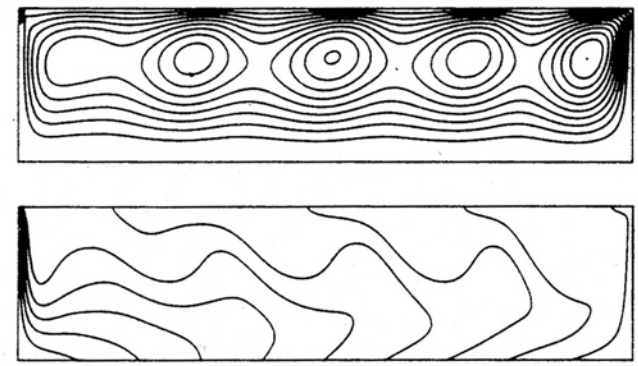

Fig. 16. Streamlines of multicellular (steady) thermocapillary convection in Pr = 4 fluid heated from the right-side. The cell axes are perpendicular to the temperature gradient. For larger Ma HTWs can travel from "cold" to "hot" (or vice versa depending on Pr) and the multicells will oscillate according to the HTW frequency [30]. The multicellular state can serve as basic state for HTWs [14, 16].

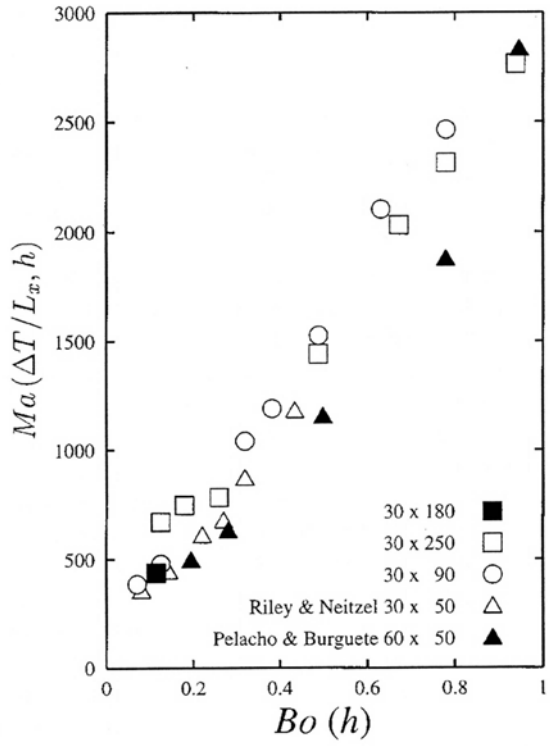

Fig. 17. The critical Ma increases with Bo, that is for increasing d, because of increasing gravitational effects (planar HTWs in extended rectangular cavities) [37].

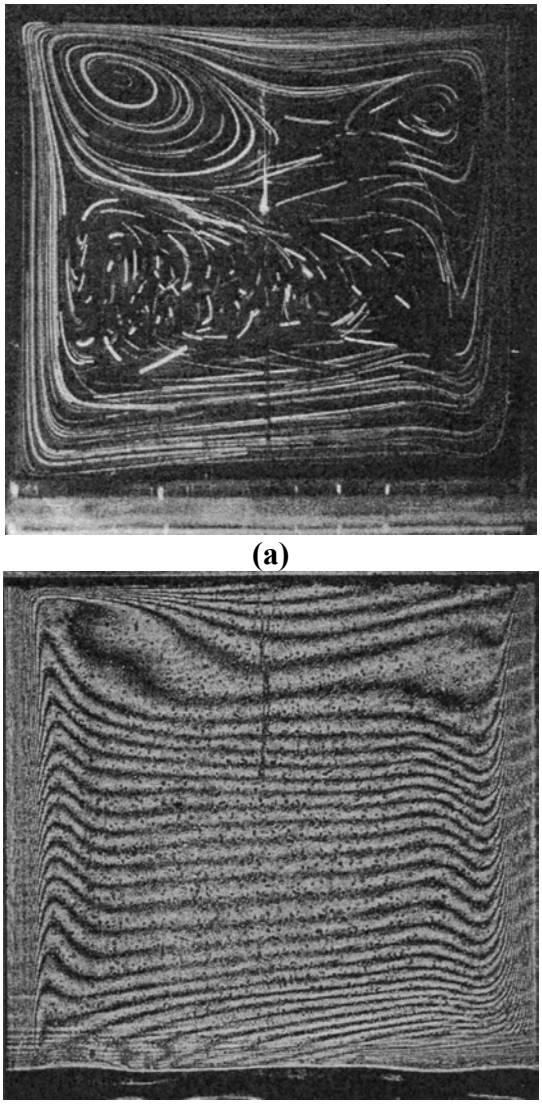

(a)

(b)

Fig. 18. (a) Streaklines and (b) isotherms by holographic interferometry in a cubic fluid cavity with L = H = 20 mm at ΔT = 4 K (Pr = 17). The cavity has a flat free surface without any menisci at its side walls [46]. Indicated is the separation of a thermocapillary convection roll with hot fluid on top of cold fluid in the bulk.

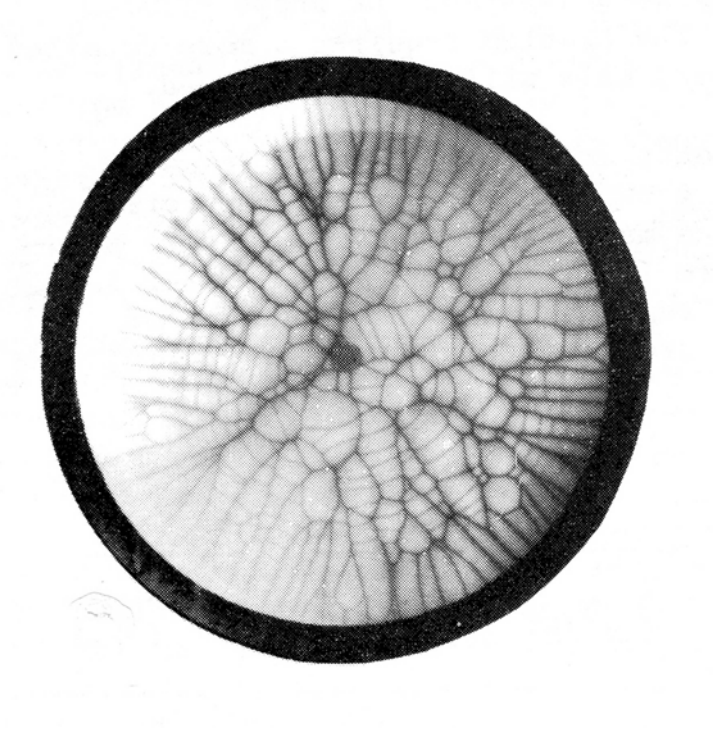

Fig. 19. Cellular convection pattern observed on Garnet melt surface (melting point ~ 1750° C) with a melt depth d > 30 mm, drifting rapidly radially inwards to the coldest spot of the surface. Note linear rolls (steady) near the heated wall also called "spokes", note cross cells between the spokes (drifting) and chaotic Bénard-like cells in the centre [55].

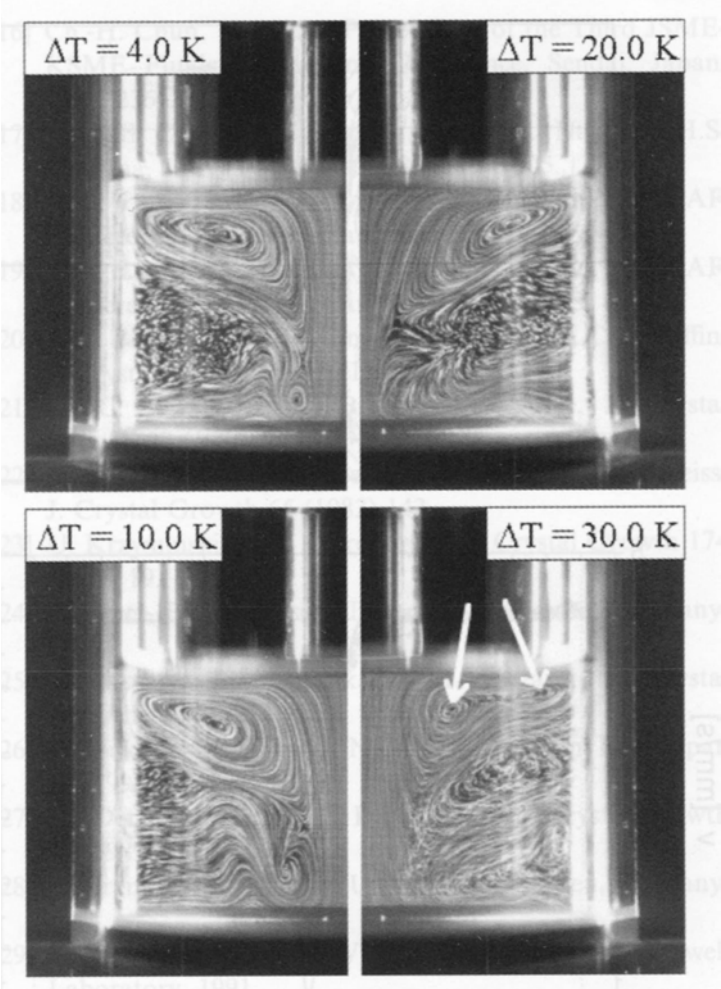

Fig. 20. Streaklines in a 40 mm ∅ crucible, liquid depth d = 20 mm, different ΔT between hot crucible and cold crystal dummy, showing the separation of the surface tension driven convection from bulk convection [51].

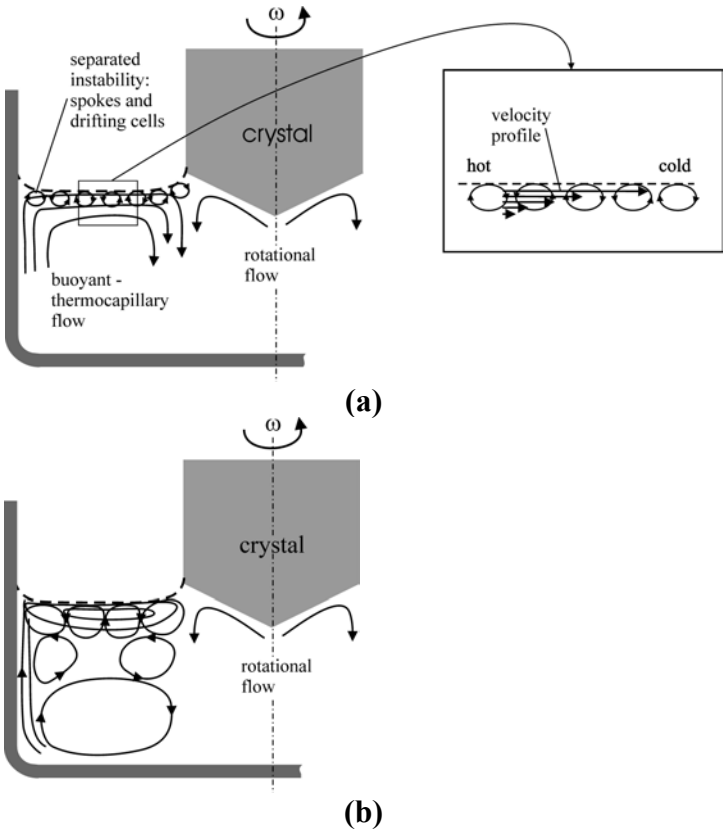

Fig. 21. The counterbalance of buoyant-thermocapillary and rotationally driven flow in a high-temperature melt (Pr >> 1). A thermocapillary-driven flow can separate from the bulk flow, balancing the rotational one. And this "linear" flow profile (a) can become instable (to Bénard-like convection cells) due to large radiative heat loss from the melt surface. This heat loss is largest near the centre of the crucible or near the crystal. The instability in form of rolls or cells can reach down to the return flow (b) if the return flow is very near the surface flow due to strong separation.

Fig. 22. Stability diagram of thermocapillary flow with inclined temperature gradient, expressed by the relation between the vertical Marangoni number Ma_v and the horizontal one, Ma_h. The line "H-F" marks the transition to oblique hydrothermal waves, line "F-E" that to transverse travelling rolls and lines 1 and 2 that to stationary longitudinal rolls [59].above the threshold.

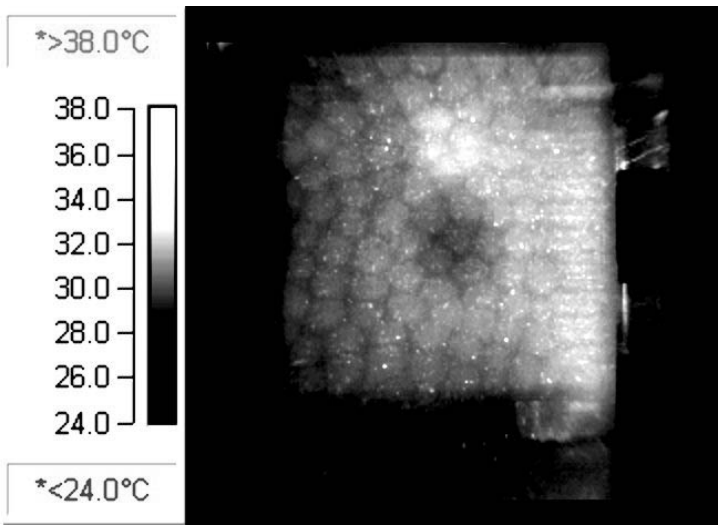

Fig. 23. Linear thermocapillary flow without return flow cooled from above (sapphire lid with temperature gradient parallel to that in the metal bottom) shows convection cells drifting with the linear flow for Ma_v above the threshold. Visualization with IR camera, IR illumination and aluminum flakes. (d = 1.34 mm, Ma_v = 12.6, Ma_v = 132, Pr = 10) [63]. In the right part of the figure (hot) Ma_v is too small for the cellular instability and linear rolls can be observed.

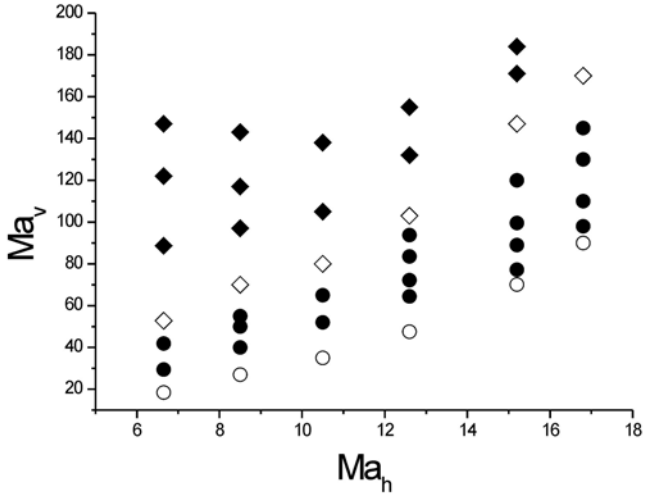

Fig. 24. Stability limits of linear thermocapillary flow cooled from above [63]. For a certain Ma_h with linear flow we find with increasing Ma_v
- ○ stable linear flow
- ● longitudinal rolls
- ◊ transition from rolls to drifting cells (guessed)
- ▪ drifting cells

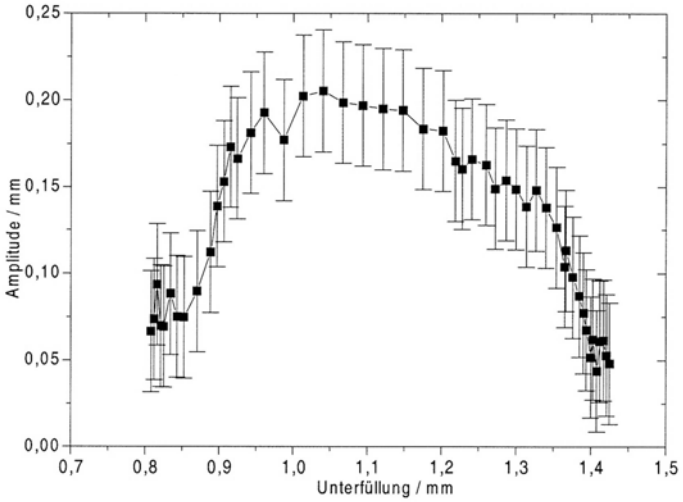

Fig. 25. The amplitude of standing surface gravity waves in a cavity with L = 20 mm, d = 20 mm, W = 41 mm, ΔT = 27.5 K when the underfilling h from a flat free surface is increased up to h = 1.4 mm. Onset at h = 0.8 mm [29].

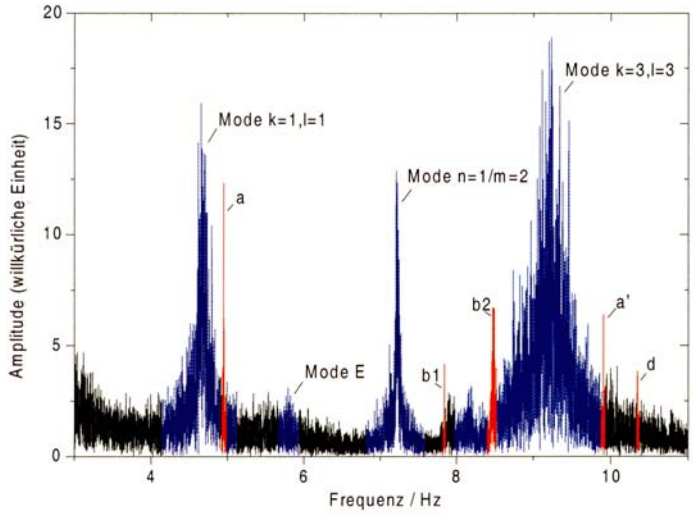

Fig. 26. Spectra of hydrodynamic instabilities in the meniscus (red) and spectra of standing surface gravity waves in a cavity (L = 20 mm, W = 41 mm, ΔT = 25 K, underfilling h = 1.5 mm). The frequencies of the hydrodynamic instabilities (e.g. "a") are near to surface waves frequencies to excite these (e.g. mode k = 1, l = 1) [29].

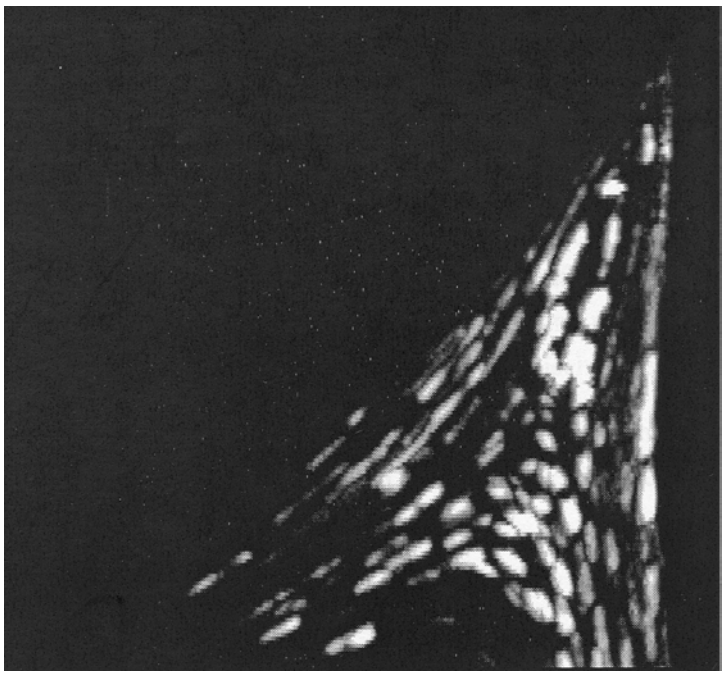

Fig. 27. Time-dependent flow in the meniscus at the cold wall (L = 12 mm, W = 41 mm, ΔT = 45.5 K, h = 1.8 mm). The thermocapillary vortex fills only the upper part of the meniscus and secondary vortices are visible below it [29].

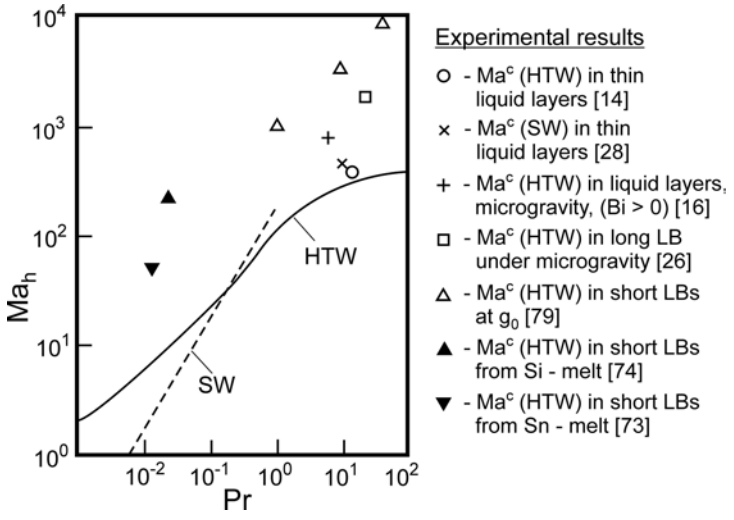

Fig.28. The measured critical Marangoni numbers in liquid bridges and layers (symbols) are generally larger than the theoretical ones (lines from[13]) but with the correct tendency. The reason for the discrepancy might be uncontrolled surface tension properties for the metallic systems (oxide impurities) and for the high-Pr liquids the "consumtion" of the largest part of the applied temperature gradient in the thermal boundary layers. The critical value measured at liquid layers with temperature gradient in the metal bottom is nearest to theory, therefore.

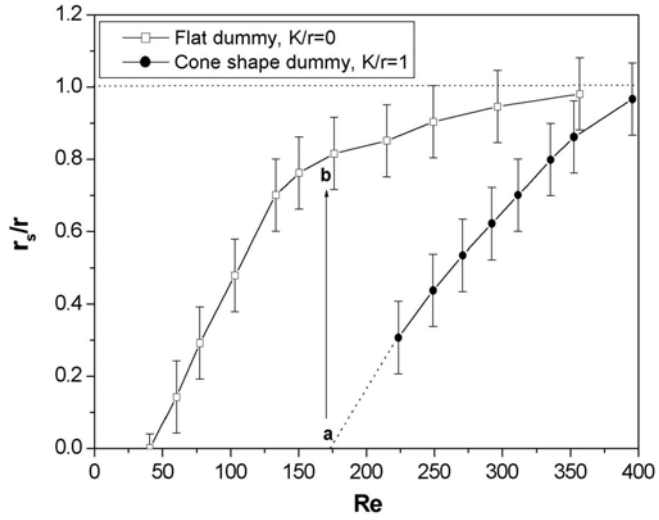

(a)

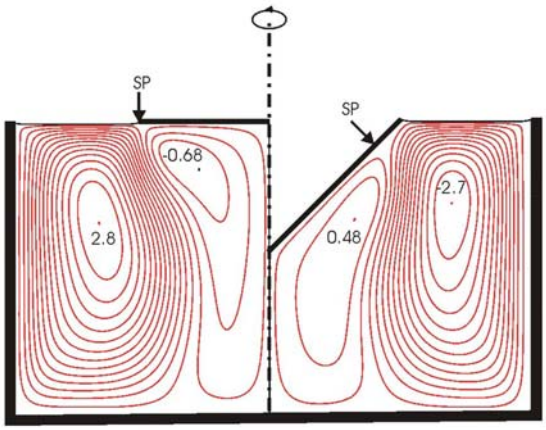

(b)

Fig. 29. The counterbalance between buoyant-thermocapillary and rotationally driven flow of a flat interface (K/r = 0) and a conically deflected one (K/r = 1) (crystal radius r, stagnation point at r_s, rotational Reynolds number $Re = 2\,\pi fr^2/\nu$).
a) Experimental result of the stagnation position for two different K/r at constant buoyant-thermocapillary flow; the flat interface needs smaller Re to shift the stagnation point to $r_s/r = 0.9$.
b) Numerical result on flow and stagnation positions (SP) for two interface shapes (flat on the left side, conical on the right side) for else unchanged boundary conditions for the flow.
Though the boundary conditions of the experiment are used for the simulation, the simulation does not show the separation of the thermocapillary flow observed in the experiments. The separation of the thermocapillary flow could increase the observed difference in the action of a flat and a conical interface [58].